Catalysis Today 201 (2013) 167–174

Contents lists available at SciVerse ScienceDirect

Catalysis Today

journal homepage: www.elsevier.com/locate/cattod

Photocatalytic and photoelectrocatalytic degradation of small biological compounds: A case study of uridine

Guiying Li[a], Yulong Zhang[a,d], Hongwei Sun[a,d], Jinbin An[a,d], Xin Nie[a,d], Huijun Zhao[b], Po-Keung Wong[c], Taicheng An[a,*]

[a] State Key Laboratory of Organic Geochemistry, Guangzhou Institute of Geochemistry, Chinese Academy of Sciences, Guangzhou 510640, China
[b] Centre for Clean Environment and Energy, Gold Coast Campus, Griffith University, QLD 4222, Australia
[c] School of Life Sciences, The Chinese University of Hong Kong, Shatin, NT, Hong Kong Special Administrative Region, China
[d] Graduate School, Chinese Academy of Sciences, Beijing 100049, China

ARTICLE INFO

Article history:
Received 5 January 2012
Received in revised form 8 March 2012
Accepted 10 March 2012
Available online 17 April 2012

Keywords:
Photocatalysis
Photoelectrocatalysis
Uridine
Degradation mechanism
Mineralization

ABSTRACT

Photocatalytic (PC) and photoelectrocatalytic (PEC) degradation of small hazardous biological compounds was accomplished by using uridine as a model compound. The net charge transfer (Q_{net}) originated from PEC degradation of uridine and blank charge transfer (Q_{blank}) due to photocatalytic oxidation of water remained constant when the light intensity increased from 20 to 40 mW/cm^2. The effect of solution pH on Q_{net} and Q_{blank} showed that the suitable pH range for this proposed analytical application is between 4 and 9. For both PC and PEC, an increase in the uridine concentration within low concentration range led to a rapid decrease in the mineralization percentage for converting organic nitrogens to both NH_3/NH_4^+ and NO_3^-. With further increase of uridine concentration to 320 μM, the PEC mineralization percentages maintained at about 85% and 56% for N oxidized to NH_3 and NO_3^-, respectively. While for PC treatment, the mineralization percentages decreased steadily. Finally, PC and PEC degradation mechanism of uridine was also clarified on the basis of intermediates identified by HPLC/MS/MS and frontier electron densities calculation. Uridine as well as the intermediates can be eventually mineralized into CO_2, H_2O and NH_3 or NO_3^- (or both) during PC and PEC degradation with enough reaction time.

1. Introduction

Besides heavy metals and organic contaminants, the pathogenic biohazard is another important group of contaminants present in aquatic environment. Microbial pathogens in drinking water and wastewater impose a serious threat on public health and safety, responsible for over 80% of disease outbreaks [1]. The removal of biohazards has therefore drawn an increasing attention to researchers in the field. In this regard, the recently reported water disinfection technique based on photocatalysis processes at illuminated nanostructured titanium dioxide (TiO_2) has attracted considerable research interests [2–6]. The major attraction of such type photocatalysis-based disinfection techniques is that the inactivation and decomposition of biohazards can be achieved in a single process without the use of toxic chemicals and producing hazardous byproducts [6,7]. Various bacterial inactivation mechanisms have been proposed by different research groups. For instance, Lu et al. [8] proposed that •OH attacks to intracellular macromolecules such as nucleic acids could lead to the cell death. A two-step inactivation mechanism involving photocatalytic (PC) decomposition of the outer membrane and disordering the cytoplasmic membrane were suggested by Sunada et al. [9]. However, the oxidative damage and decomposition of genetic material such as DNA and RNA has been recognized as a major cause of mutations and cell death in all aerobic microorganisms [10,11]. It is well known that a microbial cell is built by different classes of large biomolecules (e.g., protein, DNA and RNA). These large biomolecules consist of large numbers of basic building blocks (e.g., amino acids and nucleotides). A conjectural view of microbial cell decomposition is that the process is highly complicated as it involves an initial breaking down of the microbial cell to large biomolecules, which is further decomposed to small biological species (basic building blocks) before the mineralization is achieved. PC degradation of nucleotides is of interest due to a sensible bottom-up approach that could aid in interpreting such complex disinfection processes by investigating the degradation behaviors of basic building blocks such as uridine. Nevertheless, little has been known regarding the mechanistic steps of PC degradation of microbial cells at the molecular level. Another reason for interesting on PC degradation of uridine is because the uridine exists not only as one of the four naturally occurring nucleosides found in cellular RNA in biological species, but also as a

* Corresponding author. Tel.: +86 20 85291501; fax: +86 20 85290706.
E-mail address: antc99@gig.ac.cn (T. An).

0920-5861/$ – see front matter © 2012 Elsevier B.V. All rights reserved.
http://dx.doi.org/10.1016/j.cattod.2012.03.024

pollutant in environment resulted from sewage effluents, hospital waste, human excrements, and improper disposal of unused drugs. Such type of contaminations mainly come from the use of uridine as a versatile therapeutic agent for patients with hereditary orotic aciduria, cystic fibrosis, liver dysfunction, chemotherapy toxicity, pervasive developmental delay, schizophrenia, epilepsy, and diabetes-induced peripheral neuropathy [12,13]. Hence, it is very necessary to understand the fates, as well as the degradation patterns in the aquatic environment. However, the PC degradation of uridine has yet not been studied.

In this account, we emphasize our recent efforts to aid in the understanding the PC degradation of nucleotides using uridine as the model compound. It has been widely accepted that the application of an appropriate potential bias to a TiO_2 nanoparticulate photoanode during the PC oxidation can significantly improve the degradation efficiency of organic compounds [14–16]. The applied potential bias to timely remove the photogenerated electrons and physical separation of photoanode from the cathode are generally regarded as the major attributions for the enhanced efficiency [17,18]. For this reason, the photoelectrocatalytic (PEC) degradation of uridine was also studied. The PC and PEC degradation characteristics were compared and degradation pathways were tentatively proposed based on the degradation intermediates detected by HPLC/MS/MS and the frontier electron densities (FEDs) calculation results.

2. Materials and methods

2.1. Reagents and apparatus

Uridine (≥99%) was supplied by Sigma–Aldrich Inc. and used as received. Titanium butoxide (97%), acetonitrile (for HPLC, ≥99.9%) and sodium perchlorate (≥98.0%) were also obtained from Sigma–Aldrich Inc. All other reagents were of analytical grade and purchased from Guangzhou Chemical Reagent Co., Inc., China. Indium tin oxide conducting glass slides (ITO, 8 Ω/square) were purchased from Delta Technologies Ltd. (USA). All solutions were prepared using high purity deionized water (Millipore Corp., 18 MΩ cm).

2.2. Apparatus and methods

Both PC and PEC degradation experiments were performed under identical UV intensity using the same UV-LED/TiO_2 photoelectrochemical thin-layer cell [15]. The TiO_2 photoanode was prepared by hydrolysis of titanium butoxide according to the method described in our previous study [19]. A UV-LED (NCCU033 (T), Nichia Corporation) was used as the illumination source. The specified peak wavelength of the LED was 365 nm with a spectrum half width of 8 nm. The UV intensity was adjusted by a power supply and measured with an UV-irradiance meter (UV-A, Beijing Normal University).

As for PEC degradation experiments, a microelectrochemical system (μECS, PLAB, Changchun Institute of Applied Chemistry, Chinese Academy of Sciences, China) powered and controlled by a laptop was used for application of potential bias and current signal recording. For the exhaustive degradation experiment, a sample containing various concentrations of uridine and 2.0 M $NaClO_4$ supporting electrolyte was injected into the thin-layer cell via a precision pump before the degradation process and then subjected to PEC oxidation. For samples need HPLC analysis after PEC oxidation, a continuous sample injection mode via a precision pump during the degradation process was used. Under such conditions, the reaction time of a sample was controlled by adjusting the flow rate. A sufficient volume of the reacted sample was collected for further analyses after the system reaching its steady-state. A 2.0 M $NaClO_4$ solution was used to clean the cell between the two sample injections. PC degradation experiments were conducted under identical conditions as PEC system, except the electrochemical system was disconnected.

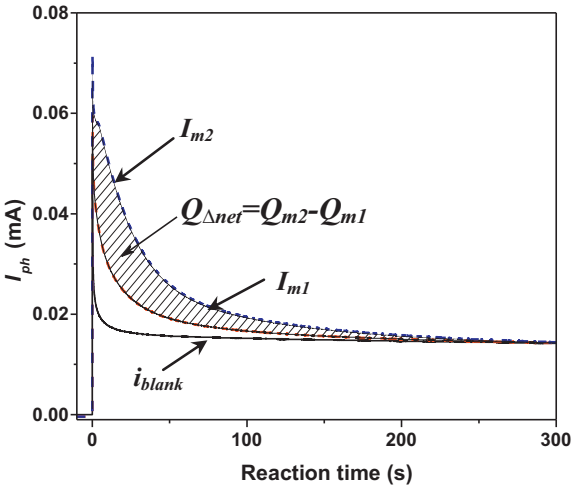

Fig. 1. Schematic illustration of charge quantification using a series of typical photocurrent profiles of the TiO_2 photoanode in the thin-layer photoelectrochemical cell of photocatalytic degradation of organic compounds.

2.3. Analysis

For PEC experiments, the extent of the mineralization was determined by measuring the charge originated from the oxidation of uridine using PeCOD™ technique [17,19]. The measured net charge transfer (Q_{net}) during the degradation was used to calculate the percentage of mineralization in accordance to:

$$\text{Mineralization}\ (\%) = \frac{Q_{net}}{Q_{th}} \times 100\%$$

where Q_{th} is the theoretically required charge transfer for complete mineralization calculated using Faraday's law, according to Eqs. (1) and (2) [15,17].

$$C_yH_mO_jN_kX_q + (2y-j)H_2O \rightarrow yCO_2 + qX^- + kNH_3 + (4y-2j+m-3k)H^+ + (4y-2j+m-3k-q)e^- \quad (1)$$

$$n_{NH_3} = 4y-2j+m-3k-q \quad (1a)$$

$$C_yH_mO_jN_kX_q + (2y-j+3k)H_2O \rightarrow yCO_2 + qX^- + kHNO_3 + (4y-2j+m+5k)H^+ + (4y-2j+m+5k-q)e^- \quad (2)$$

$$n_{NO_3^-} = 4y-2j+m+5k-q \quad (2a)$$

where N and X represents nitrogen and halogen atom, respectively. The numbers of carbon, hydrogen, oxygen, nitrogen and halogen atoms in the organic compound are represented by y, m, j, k and q. n_{NH_3} and $n_{NO_3^-}$ are the required number of electron transfer for converting N to NH_3/NH_4^+ and NO_3^-, respectively.

For PC experiments, the extent of the mineralization was also determined by measuring the charge transfer originated from the PC oxidation of organic pollutants using PeCOD™ technique [17,19]. Fig. 1 shows a set of typical photocurrent–time profiles obtained during exhaustive PC degradation of organic pollutants in

the thin-layer cell and is used to illustrate the method of the quantification of the net charge transfer (ΔQ_{net}) due to PC degradation of organic pollutants. The i_{m1} and i_{m2} represent the photocurrent profiles of the same sample solution before and after PC treatment. The photocurrent obtained from the electrolyte solution was the blank current (i_{blank}), due purely to the photocatalytic oxidation of water. Q_{m1} and Q_{m2} are net charges of the sample before and after PC degradation and calculated in accordance with:

$$Q_{m1} = \int (i_{m1})\,dt - \int (i_{blank})\,dt \quad (3)$$

$$Q_{m2} = \int (i_{m2})\,dt - \int (i_{blank})\,dt \quad (4)$$

The net charge due to PC degradation (ΔQ_{net}) can therefore be calculated as:

$$\Delta Q_{net} = Q_{m1} - Q_{m2} \quad (5)$$

which is the shaded area indicated in Fig. 1.

As aforementioned, the mineralized amount is directly proportional to ΔQ_{net}, the percentage of PC mineralization can therefore be calculated according to:

$$\text{Mineralization}\ (\%) = \frac{Q_{m1} - Q_{m2}}{Q_{th}} \times 100\% = \frac{\Delta Q_{net}}{Q_{th}} \times 100\% \quad (6)$$

The PC and PEC degradation intermediates were analyzed using an Agilent iron-trap mass spectrometer (MSD-Trap-XCT) coupled with Agilent HPLC system (1200 Series). Samples from the photocatalytic experiments were separated by the Poroshel C18 column (150 mm × 3 mm, 2.7 μm particle size). The mobile phase was 100% H_2O. The flow rate was 0.4 mL/min. The injection volume was 5 μL. The MS analysis was performed with electrospray ionization (ESI) interface both in the positive and negative ion mode with a capillary voltage of 3500 V. The nebulizer was set to 50 psi and the dry gas flow was 10 L/min. Nitrogen was used as nebulizer and dry gas. The dry gas temperature and source temperature were set at 350 and 120 °C, respectively. The mass spectrum scan ranges from 50 to 600 m/z, trap target mass 200 m/z. Absolute threshold Auto MS^2 was 50,000.

2.4. Frontier electron densities and point charges calculations

The molecular orbital (MO) calculations were carried out by using Gaussian 03 program (Gaussian, Inc.) at the single determinant (HF/3–21) level with the optimal conformation having minimum energy obtained at the B3LYP/6–31G* level. And then the FEDs of the highest occupied molecular orbital (HOMO) and the lowest unoccupied molecular orbital (LUMO) were calculated. The values of $2FED^2_{HOMO}$ and $(FED^2_{HOMO} + FED^2_{LUMO})$ were obtained to predict the reaction sites for electron extraction and radical attack, respectively [20,21]. All the calculations were performed on a personal computer.

3. Results and discussion

3.1. The effect of reaction time

Fig. S1 shows a series of typical photocurrent–time profiles of the TiO_2 photoanode obtained from the PEC degradation of samples containing different uridine concentrations in the thin-layer photoelectrochemical cell under a constant applied potential bias of +0.30 V (versus Ag/AgCl) in a 2.0 M $NaClO_4$ electrolyte solution with UV illumination (light intensity: 20 mW/cm^2). A near zero current was observed before the UV illumination was switched on. However, when the UV illumination was turned on, instantaneous transient photocurrent spikes were observed due to the photocatalytic oxidation of the adsorbed water and/or uridine accumulated at the electrode surface during the dark period. The photocurrent decayed rapidly within the initial few seconds and attained their steady-state (approximately 50 s for water and 250 s for uridine containing samples). These observations suggest that the measured current is due purely to the photocatalytic process rather than the direct electrochemical reactions because the potential bias is too low for direct electrochemical oxidation of uridine.

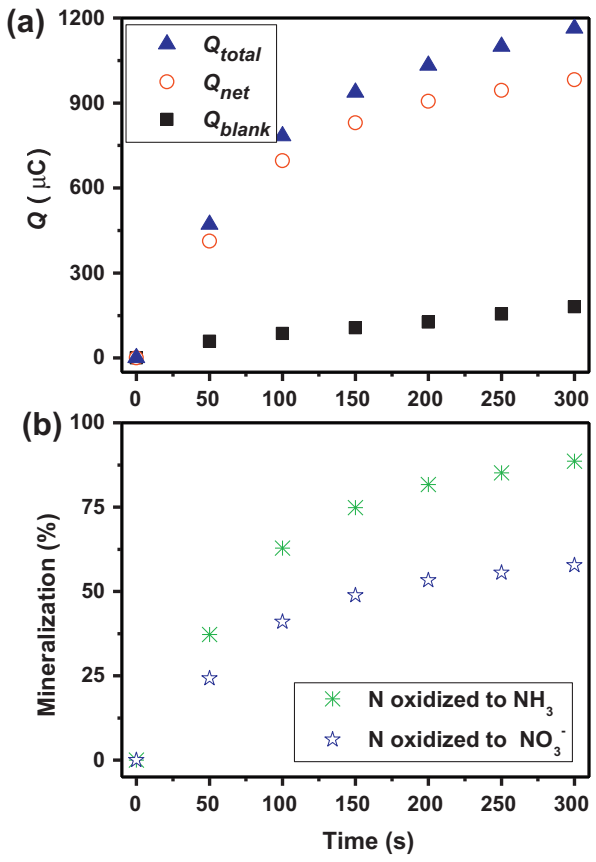

Fig. 2. Effect of reaction time on (a) Q_{total}, Q_{net} and Q_{blank}, (b) mineralization for photoelectrocatalytic oxidation of 200 μM uridine and supporting electrolyte solution.

Fig. 2a demonstrates the plots of the measured Q_{blank} (the charge originated from the oxidation of water, and can be obtained by integration of photocurrents, i_{blank} with time), Q_{net} and Q_{total} (the charge originated from the oxidation of water and uridine) against the reaction time in presence of 200 μM uridine. It can be found that the Q_{blank} increases from 0 to 59 μC during the first 50 s when the UV illumination was switched on, and then it increases very slowly with further increase of the UV irradiation time. Whereas, the Q_{total} and especially Q_{net} increased linearly with reaction time up to approximately 150 s before leveling off. All these results revealed that the PEC degradation reaction of different concentrations of uridine could be finished within 300 s. From the Fig. 2b, it can be seen that, with the increase of the reaction time from 0 to 150 s, the mineralization percentage increased from 0% gradually to 74.9% at first, and then leveled off at 88.6% (300 s) when the nitrogen atoms in uridine were converted to NH_3. According to Eqs. (1) and (2), in a PEC degradation process, the nitrogen atoms in uridine can be converted to NH_3, NO_3^- or both. It is obvious that the extent of mineralization will be strongly influenced by the final mineralization products of the organic nitrogens, since the required numbers of electron transfer for converting N to NH_3 and NO_3^- are different. Each uridine molecule needs more 16 e^- to convert N to NH_3

than to NO_3^-. And as the nitrogen atoms in uridine were converted NO_3^-, the mineralization percentage increased from 0% gradually to 48.8% first, and then leveled off at 57.8%. Therefore, the reaction time of 300 s was chosen for subsequent experiments.

3.2. The effect of light intensity

It is well known that the incident light intensity determines the rate of photohole generation, consequently controls the rate of interfacial reactions [22,23]. Therefore, the effect of light intensity on PEC degradation of uridine was investigated. All experiments were performed under exhaustive degradation conditions with a constant saturated applied potential bias of +0.30 V in 2.0 M $NaClO_4$ solution containing 200 μM of uridine. The applied light intensity varied from 10 to 50 mW/cm^2.

Fig. S2a shows the plots of the measured Q_{blank}, Q_{net} and Q_{total} against the light intensity in presence of 200 μM uridine. It was found that the measured Q_{net} and Q_{total} increased as the light intensity increased from 10 to 20 mW/cm^2, suggesting the increase of the rate of photohole generation, because the light intensity was the limiting step of the overall process. And the mineralization percentage increased from 71.7% gradually to 88.6% within this test light intensity range, as the nitrogen atoms in uridine were converted to NH_3 (Fig. S2b). The Q_{total} and Q_{blank} obtained from uridine and water oxidation were found to increase when the light intensity was further increased to 40 mW/cm^2. However, the Q_{net} originated from the oxidation of uridine, was found to be essentially constant with a very slight fluctuation within the light intensity range tested, revealing the increase of Q_{total} was caused by the increase of Q_{blank} at higher light intensity. That is, the Q_{net} was independent of the light intensity in this intensity range. The mineralization percentage maintained at about 85%, as N in uridine was converted to NH_3. This can be interpreted that the increase of light intensity (injection of more photons) leads to generation of more photoholes and subsequently enhance oxidation rate, when sufficient TiO_2 catalyst is present [24]. The reaction time is inversely proportional to the light intensity [25]. With further increase of the light intensity from 50 to 60 mW/cm^2, the Q_{blank} rose steadily, while the measured Q_{net} decreased gradually. The mineralization percentage decreased from 74.4% to 62.5% for N oxidized to NH_3, and from 48.5% to 40.8% for N oxidized to NO_3^-. This is probably because with extremely high UV illumination intensity, air bubbles might be produced via the water splitting, or photocorrosion of the TiO_2 semiconductor electrode is associated, both of which will affect the analytical signal seriously. When all the factors were considered, a relatively lower (but sufficient) light intensity of 20 mW/cm^2 was chosen for all subsequent experiments.

3.3. The effect of pH

The solution pH affects the speciation of surface functional groups of the semiconductor electrode as well as the flat band potential or band edge potential of oxide semiconductors [26,27]. In addition, it can also affect the chemical forms of organic compounds in the solution. All of these pH dependent factors may also influence the PEC degradation of uridine.

Therefore, the effect of the solution pH on the Q_{total}, Q_{net} and Q_{blank} in presence of uridine was then investigated (Fig. 3a). All the experiments were carried out in 2.0 M $NaClO_4$ solution containing 0.20 mM uridine, under a constant light intensity of 20 mW/cm^2 and an +0.30 V applied potential bias. The pH effect was examined within the range of pH 4–9, as TiO_2 thin film becomes unstable under excessive acidic or alkaline conditions [28]. Exceeding acidic solution can seriously damage the ITO conductivity [25], and too alkaline solution will substantially increase the amount of ⟩TiO— surface groups of the TiO_2 electrode that favors the trapping of

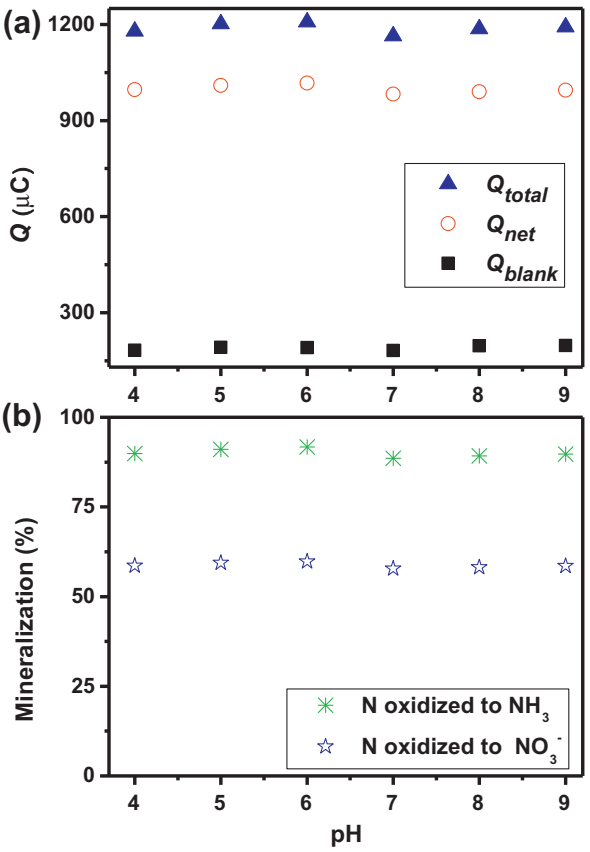

Fig. 3. Effect of pH on (a) Q_{total}, Q_{net} and Q_{blank}, (b) mineralization for photoelectrocatalytic oxidation of 200 μM uridine as well as supporting electrolyte solution.

photoholes, leading to a higher photocatalytic activity towards water oxidation [29,30]. From Fig. 3, it can be found that the measured Q_{total}, Q_{net} and Q_{blank} (Fig. 3a), as well as the mineralization percentage (Fig. 3b) remained constant when the pH increased from 4 to 9. In other words, they were independent of pH variations within the tested pH range. Based on these observations, the suitable pH range for the TiO_2 photoanode should be between pH 4 and 9.

3.4. The effect of uridine concentration

Under optimized condition, the effect of small biological organic pollutants on the Q_{net} was investigated using uridine as model organics. All experiments were performed under exhaustive degradation conditions with a constant UV light intensity of 20 mW/cm^2 in a 2.0 M $NaClO_4$ solution containing different concentration uridine at nature pH value (pH 5.6). The applied potential bias was fixed at +0.30 V versus a saturated Ag/AgCl reference electrode.

As mentioned, Fig. S1 shows a set of typical photocurrent–time profiles of the TiO_2 photoanode obtained from the PEC degradation of uridine in different concentrations. Fig. S3 also illustrates a set of typical photocurrent–time profiles obtained from uridine samples before and after PC treatment. These photocurrent profiles are used to calculate the mineralization efficiencies of PEC and PC treated samples by measuring the amount of electrons lost during the PEC and PC treatment in accordance with Eq. (6).

Fig. 4 shows the plots of the mineralization percentage of PC and PEC treated uridine against the uridine concentration for organic nitrogen mineralized to NH_3/NH_4^+ and NO_3^-. All samples were photocatalytically or photoelectrocatalytically treated for 300 s under the light intensity of 20 mW/cm^2 UV. For both PC and PEC,

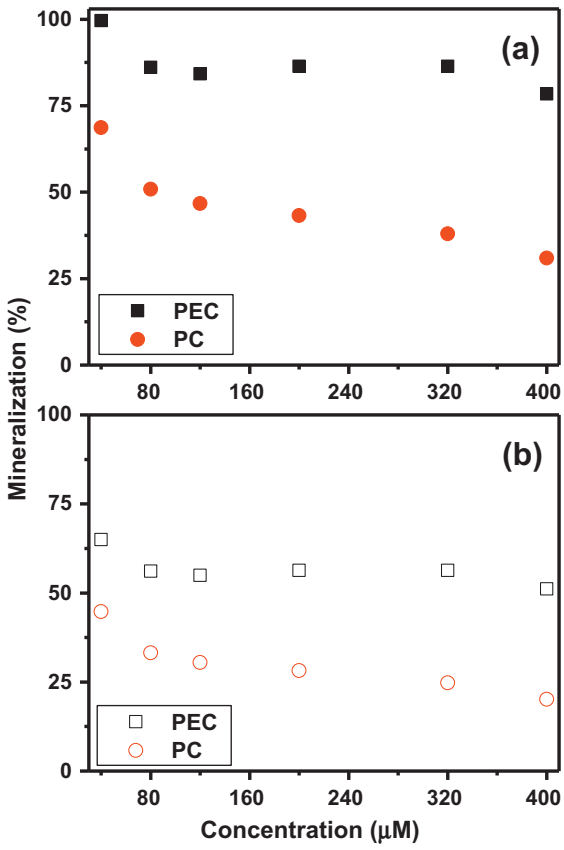

Fig. 4. Photocatalytic and photoelectrocatalytic degradation of uridine, the correlation between the percentage mineralization and uridine concentration: (a) for N oxidized to NH_3 and (b) to NO_3^-.

an increase in the uridine concentration within low concentration range led to a rapid decrease in the mineralization percentage for converting organic nitrogen to both NH_3/NH_4^+ and NO_3^-. For instance, the PC and PEC mineralization percentages dropped from 68.7% to 50.9% and 99.6% to 86.1%, respectively, for N oxidized to NH_3, and from 44.8% to 33.2% and 65.0% to 56.2%, respectively, for N oxidized to NO_3^-. With the increase of the uridine concentration further to 320 μM, the PEC mineralization percentages maintained at about 85% and 56% for N oxidized to NH_3 and NO_3^-, respectively. While for the PC treatment, the mineralization percentages decreased steadily from 46.7% to 30.9% and 30.5% to 20.2% for N oxidized to NH_3 and NO_3^-, respectively. This is due to that the PEC technology possessed higher oxidation ability than that of PC even at higher organics concentration. In general, the mineralization efficiencies of the PEC treated system converting to both NH_3/NH_4^+ and NO_3^- were found to be much higher than that of PC treated system under the same experimental conditions, suggesting a superior PEC degradation capability.

Therefore, the effect of uridine concentration on the differences between the extent of PEC and PC mineralization were also quantitatively evaluated by plotting the PEC and PC mineralization ratio against the C_{eq} (equivalent electron concentration for organic nitrogens mineralized to NH_3 and NO_3^-) (Fig. 5). The use of C_{eq} is a more meaningful comparison among different organics because such a noncharacteristic concentration unit represents the electron demands for complete mineralization, regardless of their chemical structures and electron transfer numbers [31]. It can be found that a linear relationship was obtained, revealing that the superiority (in terms of mineralization efficiency) of PEC method over the PC method increases as the uridine concentration increases. In addition, the slope of the curve quantifies the degree of the superiority of

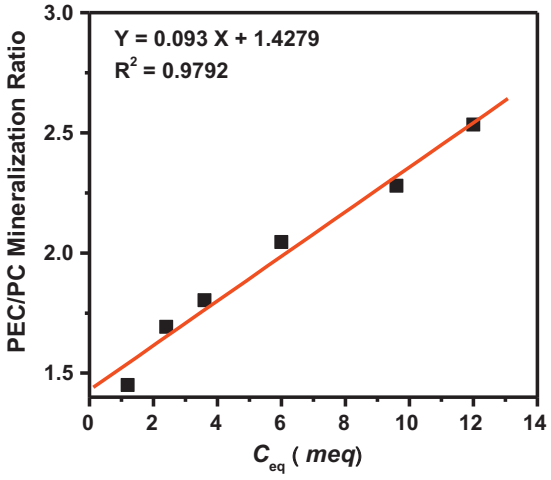

Fig. 5. A plot of PEC to PC mineralization ratio against C_{eq} (N oxidized to NH_3) for uridine.

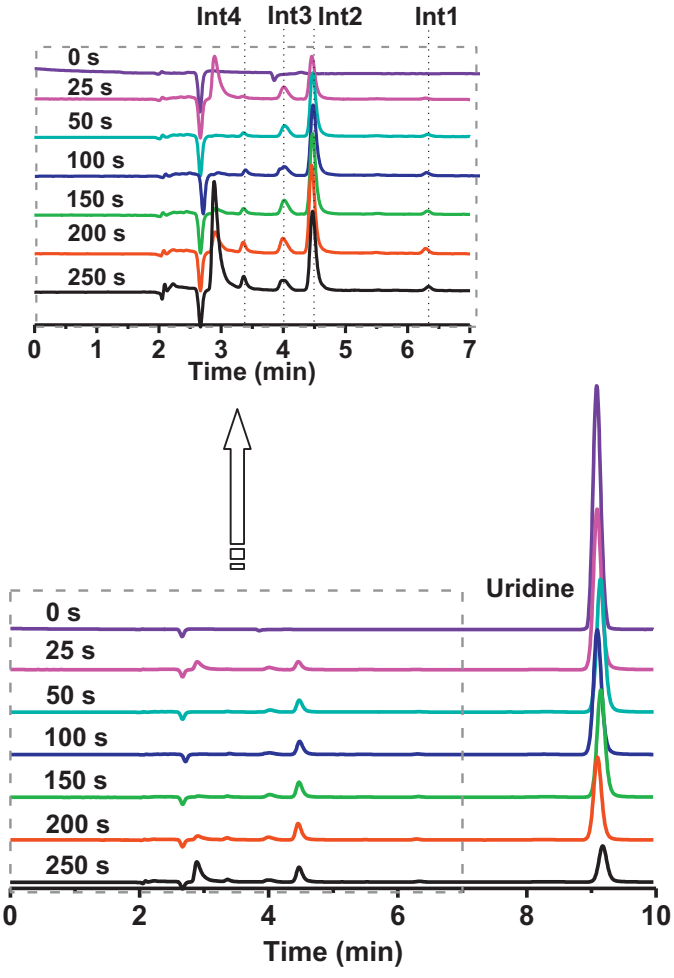

Fig. 6. The HPLC chromatograms obtained for PEC treated uridine samples at different reaction intervals under 20 mW/cm² UV intensity. Initial concentration: 400 μM; applied potential bias for PEC: +0.30 V vs. Ag/AgCl; retention time: t_R(*uridine*) = 9.1 min; t_R(*Intermediate 1*) = 6.3 min; t_R(*Intermediate 2*) = 4.5 min; t_R(*Intermediate 3*) = 4.0 min; t_R(*Intermediate 4*) = 3.4 min.

Table 1
Frontier electron densities (FEDs) on atoms of uridine calculated by using Gaussian 03 program.

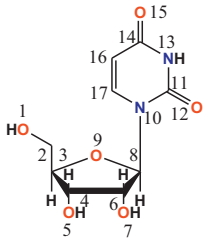

Uridine

Atom	$2FED^2_{HOMO}$ h^+	$FED^2_{HOMO} + FED^2_{LUMO}$ $^{\bullet}OH$	Atom	$2FED^2_{HOMO}$ h^+	$FED^2_{HOMO} + FED^2_{LUMO}$ $^{\bullet}OH$
O^1	0.0009	0.0020	N^{10}	**0.3993**	0.2849
C^2	0.0009	0.0099	C^{11}	0.0098	0.0295
C^3	0.0009	0.0037	O^{12}	0.0768	0.0500
C^4	0.0070	0.0083	N^{13}	0.0015	0.0833
O^5	0.0051	0.0027	C^{14}	0.0029	0.1544
C^6	0.0370	0.0270	O^{15}	0.1605	0.1920
O^7	0.0093	0.0076	C^{16}	**0.4541**	**0.4189**
C^8	0.0224	0.0209	C^{17}	0.1502	**0.6066**
O^9	0.0116	0.0077			

the PEC method over the PC method in respect to the concentration change.

3.5. Photocatalytic and photoelectrocatalytic degradation intermediates and mechanism

The PC and PEC degradation intermediates of uridine were detected and identified by the HPLC/MS/MS. Figs. 6 and S4 showed the HPLC chromatogram of uridine being degraded by PC and PEC at different degradation time. For samples without treatment, an absorption peak (uridine) with a retention time (t_R) of 9.1 min, signifying the original uridine molecule, was observed. For the confirmation of uridine, its fragmentation behavior was studied by MS^2 measurement. The spectrum of parental ion of uridine (MW = 244.2) $[M+H]^+$ generated one abundant ion at m/z 113 (Fig. S5). The fragment ion at m/z 113 corresponded to $[M+H-H-(C=O)-(CH_2)-(CHOH)_3-H]^+$. For the PC and PEC treated samples, the concentration of the uridine decreased gradually

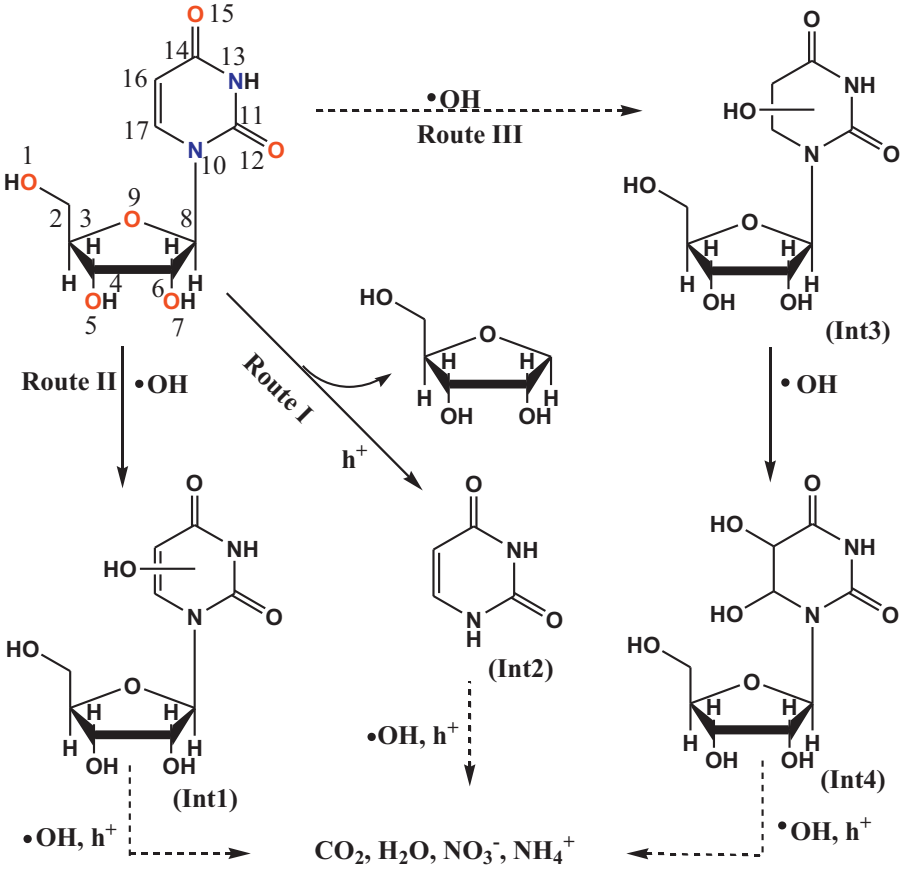

Fig. 7. Proposed photoelectrocatalytic degradation pathway for uridine.

with the increase of the treatment time, and it can be obviously found that the peak of uridine for the PEC treatment dropped more swiftly at the same time intervals. In terms of their concentrations in reaction mixtures, one dominant intermediate peak (Intermediate 2, t_R = 4.5 min), one minor intermediates (Intermediate 3, t_R = 4.0 min) and two very minor intermediates (Intermediate 1 and Intermediate 4, t_R = 6.3 and 3.4 min, respectively) were recorded for both PC and PEC degradation. It is noted that all four intermediates were more hydrophilic than uridine, which might be monohydroxylated or dihydroxylated intermediates as a result of •OH attack on C16 and/or C17 (see $FED^2_{HOMO} + FED^2_{LUMO}$ value from Table 1), and the concentration of intermediate 2 in the reaction mixture was increased as the treatment time increased.

Therefore, the MS^2 identification spectra of all intermediates after PC and PEC degradation of uridine was also carried out, and the retention times, structures as well as the characteristic fragment ions of them, with uridine are summarized in Table S1. The MS^2 spectrum in the positive ion mode of intermediate 1 with *m*/*z* 261 yielded the fragment ions corresponding to $[M+HH_2O]^+$ at *m*/*z* 243, $[M+H{-}NH_2{-}(C{=}O){-}(CHOH){=}(CH_2)]^+$ at *m*/*z* 174, and $[M+H{-}H{-}(C{=}O){-}(CH_2){-}(CHOH)_3{-}H]^+$ at *m*/*z* 129 (Fig. S6a). The MS^2 spectrum of intermediate 2 gives three significant *m*/*z* values: 96, 85, and 70 (Fig. S6b). The fragment ion at *m*/*z* 96 was corresponding to $[M+H{-}O]^+$, *m*/*z* 85 to $[M+H{-}(C{=}O)]^+$, and *m*/*z* 70 to $[M+H{-}NH_2{-}(HC{=}O)]^+$. The MS^2 spectrum of intermediate 3 at *m*/*z* 285 ($[M+Na]^+$), owing to the presence of sodium ion in reaction solution employed as the supporting electrolyte, yields the fragment ions corresponding to $[M+Na{-}H_2O{-}2H]^+$ at *m*/*z* 265, and $[M+Na{-}H{-}(C{=}O){-}(CH_2){-}(CHOH)_3{-}H]^+$ at *m*/*z* 131 (Fig. S6c). While the MS^2 spectrum of intermediate 4 at *m*/*z* 301 ($[M+Na]^+$) also yields the fragment ions corresponding to $[M+Na{-}H_2O]^+$ at *m*/*z* 283, and $[M+Na{-}(CH_2){-}(CHOH)_3{-}H]^+$ at *m*/*z* 198 (Fig. S6d). In addition, all of the intermediates except intermediate 2 were also double confirmed by MS^2 spectra in the negative ion mode (Fig. S7).

Fig. 7 is a proposed PC and PEC degradation pathway of uridine from the collected information from the identified intermediates and the calculated data of the FEDs and point charges (Table 1). This is because that theoretically calculated FEDs have been recognized as a useful tool for predicting initial reaction step [20,21]. According to the concentration change of intermediates (Figs.6 and S4), the Route I is considered as the major pathway, and uracil (Intermediate 2), which is one of the essential nucleotide bases and more basic building block of uridine, was possibly produced by h^+ attacking at N^{10} atom and broke $N^{10}{-}C^8$ bond with the loss of a ribofuranose group. This result can be confirmed by the calculated FEDs results, it can be found that the higher $2FED^2_{HOMO}$ values were obtained for N^{10} (0.3993) and C^{16} (0.4541) indicating the initial h^+ attacks are likely to occur on a nitrogen atom and a double-bonded carbon atom that is connected to a ribofuranose and a carbon atoms with —C=C—. For the Route II, the •OH can attack C^{16} or C^{17} atom, and produce a monohydroxylated intermediate (Intermediate 1). While for the Route III, the •OH attack of C^{16} or C^{17} atom lead to double bond $-C^{16}{=}C^{17}-$ breaking and with addition of a hydroxyl on C^{16} or C^{17} atom to form intermediate 3, which was subsequently oxidized to intermediate 4 with another hydroxyl radical addition on C^{17} or C^{16} atom of the intermediate 3 molecule. It is worth mentioning that, the calculated $(FED^2_{HOMO} + FED^2_{LUMO})$ values also confirmed our proposed pathway, which indicate the C^{16} (0.4189) and C^{17} (0.6066) are likely to be the initial reaction sites by the •OH attacks. Finally, the rings of all intermediates will cleaved and be fully mineralized into CO_2, H_2O and NH_3/NO_3^- during the PC and PEC degradation with further increase of the reaction time.

4. Conclusions

The PC and PEC degradation of uridine was carried out in a UV-LED/TiO_2 thin-layer photoelectrochemical cell. The Q_{net} was independent of light intensity when the light intensity increased from 20 to 40 mW/cm^2. The effect of solution pH on Q_{net} showed that the suitable pH range is between 4 and 9. For uridine mineralization, PEC method possesses higher degradation efficiency than PC method. An increase in the uridine concentration within low concentration range led to a rapid decrease in the PC and PEC mineralization percentage for converting N to both NH_3/NH_4^+ and NO_3^-. With further increase of uridine concentration, the PEC mineralization percentages maintained steadily. While for PC treatment, the mineralization percentages decreased gradually. In addition, the PC and PEC degradation mechanisms of uridine were also proposed based on the intermediates detected by HPLC/MS/MS as well as the FEDs calculation data. Four major intermediates were produced and identified during PC and PEC degradation of uridine process. The hydrophilicity characteristics of the PC produced intermediates are the same as those of PEC produced intermediates. The theoretically calculated $2FED^2_{HOMO}$ and $FED^2_{HOMO} + FED^2_{LUMO}$ values suggest that the initial reaction sites agreed well with the experimental results. The direct photohole oxidation (major pathway) leading to the cleavage of glycosidic bond and the hydroxylation addition reaction (minor pathway) on the pyrimidine ring are the two main initial steps for PC and PEC degradation of uridine. The data and insights presented here may shed new light on PC and PEC oxidation reactions of uridine as well as other small biological compounds, and should facilitate the understanding of PC and PEC disinfection and decomposition mechanisms of the pathogenic biohazards by using bottom-up strategy.

Acknowledgments

This is contribution no. IS-1478 from GIGCAS. Financial supports from NSFC (nos. 21077104 and 40973068), the Combination Project of Production, Studying and Research of Guangdong Province, China (20100908), Knowledge Innovation Program of GIG, CAS (GIGCX-10-01), and a research grant of General Research Fund (GRF476811) to P.K. Wong from the Research Grant Council of Hong Kong SAR Government.

Appendix A. Supplementary data

Supplementary data associated with this article can be found, in the online version, at doi:10.1016/j.cattod.2012.03.024.

References

[1] J.N. Ryan, R.W. Harvey, D. Metge, M. Elimelech, T. Navigato, A.P. Pieper, Environ. Sci. Technol. 36 (2002) 2403–2413.
[2] A. Markowska-Szczupak, K. Ulfig, A.W. Morawski, Catal. Today 169 (2011) 249–257.
[3] G.Y. Li, X.L. Liu, H.M. Zhang, T.C. An, S.Q. Zhang, A.R. Carroll, H.J. Zhao, J. Catal. 277 (2011) 88–94.
[4] H.A. Foster, I.B. Ditta, S. Varghese, A. Steele, Appl. Microbiol. Biotechnol. 90 (2011) 1847–1868.
[5] O.K. Dalrymple, E. Stefanakos, M.A. Trotz, D.Y. Goswami, Appl. Catal. B: Environ. 98 (2010) 27–38.
[6] T. Matsunaga, R. Tomoda, T. Nakajima, H. Wake, FEMS Microbiol. Lett. 29 (1985) 211–214.
[7] P.A. Christensen, T.P. Curtis, T.A. Egerton, S.A.M. Kosa, J.R. Tinlin, Appl. Catal. B: Environ. 41 (2003) 371–386.
[8] Z.X. Lu, L. Zhou, Z.L. Zhang, W.L. Shi, Z.X. Xie, H.Y. Xie, D.W. Pang, P. Shen, Langmuir 19 (2003) 8765–8767.
[9] K. Sunada, T. Watanabe, K. Hashimoto, Environ. Sci. Technol. 37 (2003) 4785–4789.
[10] G. Gogniat, S. Dukan, Appl. Environ. Microbiol. 73 (2007) 7740–7743.
[11] S. Bjelland, E. Seeberg, Mutat. Res. 531 (2003) 37–80.
[12] M.E. Weinberg, M.C. Roman, P. Jacob, M. Wen, P. Cheung, U.A. Walker, K. Mulligan, M. Schambelan, PLoS ONE 6 (2011) e14709.

[13] M.G. Williams, J. Palandra, E.M. Shobe, Biomed. Chromatogr. 17 (2003) 215–218.
[14] K. Vinodgopal, I. Bedja, P.V. Kamat, Chem. Mater. 8 (1996) 2180–2187.
[15] H.J. Zhao, D.L. Jiang, S.Q. Zhang, W. Wen, J. Catal. 250 (2007) 102–109.
[16] G.Y. Li, T.C. An, X.P. Nie, G.Y. Sheng, X.Y. Zeng, J.M. Fu, Z. Lin, E.Y. Zeng, Environ. Toxicol. Chem. 26 (2007) 416–423.
[17] H.J. Zhao, D.L. Jiang, S.Q. Zhang, K. Catterall, R. John, Anal. Chem. 76 (2004) 155–160.
[18] P.A. Mandelbaum, A.E. Regazzoni, M.A. Blesa, S.A. Bilmes, J. Phys. Chem. B 103 (1999) 5505–5511.
[19] S.Q. Zhang, D.L. Jiang, H.J. Zhao, Environ. Sci. Technol. 40 (2006) 2363–2368.
[20] X. Zhang, F. Wu, X.W. Wu, P.Y. Chen, N.S. Deng, J. Hazard. Mater. 157 (2008) 300–307.
[21] T.C. An, H. Yang, G.Y. Li, W.H. Song, W.J. Cooper, X.P. Nie, Appl. Catal. B: Environ. 94 (2010) 288–294.
[22] M.R. Hoffmann, S.T. Martin, W.Y. Choi, D.W. Bahnemann, Chem. Rev. 95 (1995) 69–96.
[23] A.J. Hoffman, G. Mills, H. Yee, M.R. Hoffmann, J. Phys. Chem. 96 (1992) 5540–5546.
[24] D.L. Jiang, H.J. Zhao, S.Q. Zhang, R. John, J. Phys. Chem. B 107 (2003) 12774–12780.
[25] S.Q. Zhang, L.H. Li, H.J. Zhao, G.Y. Li, Sens. Actuat. B: Chem. 141 (2009) 634–640.
[26] D.L. Jiang, H.J. Zhao, S.Q. Zhang, R. John, G.D. Will, J. Photochem. Photobiol. A: Chem. 156 (2003) 201–206.
[27] N. Chandrasekharan, P.V. Kamat, J. Phys. Chem. B 104 (2000) 10851–10857.
[28] S.Q. Zhang, H.J. Zhao, D.L. Jiang, R. John, Anal. Chim. Acta 514 (2004) 89–97.
[29] D.L. Jiang, H.J. Zhao, Z.B. Jia, J.L. Cao, R. John, J. Photochem. Photobiol. A: Chem. 144 (2001) 197–204.
[30] J. Rappich, J.K. Dohrmann, J. Phys. Chem. 93 (1989) 5261–5264.
[31] D.L. Jiang, S.Q. Zhang, H.J. Zhao, Environ. Sci. Technol. 41 (2007) 303–308.